Magnetically Assembled Multiwalled Carbon Nanotubes on Ferromagnetic Contacts†

Sandip Niyogi,[‡,||] Carlos Hangarter,[§] Ramesh M. Thamankar,[⊥] Yueh-Feng Chiang,[⊥] Roland Kawakami,[||,⊥] Nosang V. Myung,*[,§,||] and Robert C. Haddon*[,‡,§,||]

Department of Chemistry, Department of Chemical and Environmental Engineering, Center for Nanoscale Science and Engineering, and Department of Physics, University of California, Riverside, California 92521

Received: June 29, 2004; In Final Form: July 31, 2004

A facile method for assembling carbon nanotubes (CNT) on ferromagnetic metal contacts is described. Multiwalled carbon nanotubes (MWNT) with a magnetic cap were fabricated by thermally evaporating nickel on top of a vertical array of MWNTs grown on silicon. Magnetic interaction between the magnets on the nanotubes and lithographically patterned ferromagnetic electrodes caused the relative alignment and directed placement of nanotubes. The lithographically patterned electrodes were further modified using electrochemical deposition to form asymmetric ferromagnetic electrodes as well as improve the electrical and magnetic interactions at the contacts. MWNTs thus assembled showed characteristics that have been established for various nanotube device configurations. This validates the assembling technique for exploring charge- and spin-based electronic devices.

Introduction

Nanowires and nanotubes are attractive nanostructured materials for electronic, optoelectronic, and sensor applications because of their unique properties. The directional placement of immobilized nanowires and nanotubes in aligned geometries on electrodes is important for mechanical and electromechanical studies and represents a critical step toward the creation of high-density devices.[1] Current methods for controlling the directionality and placement of nanowires and nanotubes include electric field alignment during growth or post-growth,[2,3] microfluidic alignment of semiconductor nanowires followed by e-beam lithography to form contacts,[4−6] growth of nanowire arrays on a selectively etched superlattice template followed by manual transfer to the desired substrates,[7] and magnetic alignment using magnetic interactions between metallic nanowires with attached nanomagnet and ferromagnetic contacts.[8]

Individual, covalently bonded molecules provide a unique opportunity to assemble high-density and low-power electronic circuitry. Carbon nanotubes have a covalently bonded structure which controls their unique electronic and magnetic properties.[9−13] The observation of ballistic conductance,[14] together with the demonstration of spin-polarized transport,[15] indicates that carbon nanotubes are promising materials for spin-based electronic devices.[16,17] The use of ferromagnetic contacts has enabled spin injection into organic semiconductors[18,19] and metals.[20]

MWNTs and single-walled carbon nanotubes (SWNTs) can be grown as vertical arrays on substrates under suitable chemical vapor deposition (CVD) conditions.[21−24] The length, diameter, and growth rates are dependent on the substrate, catalyst, carbon source, and the growth temperature. The electronic transport properties of an MWNT is dependent on the structure of the outermost shell.[25,26] When allowed to grow at certain densities such that the length of the nanotubes can be supported by a collective crowding effect, MWNTs grow with the transition-metal catalyst pinned at one end of the nanotube as a nanoparticle of diameter comparable to that of the MWNT. When grown in this configuration, the ends of the carbon nanotubes are accessible for asymmetric modification, one of the necessary requirements for directed assembly.

In previous studies, MWNTs grown from Fe showed negative magnetoresistance on Cr contacts while the contact resistance did not change up to applied magnetic fields of 5 T,[27] and the magnetization behavior of ∼70 nm Fe particles attached to MWNTs indicated that it would be possible to generate very strong coercive fields of 2.5 kOe with Fe particles <20 nm in diameter.[28] Recent work has demonstrated magnetoresistance effects in ferromagnetically contacted CNTs in various configurations.[15,27,29−32] While carbon nanotubes have been aligned horizontally on substrates using various techniques, both during growth[2,33] and post growth,[34−38] using an external weak field to achieve this has the advantage of tailoring the directionality of assembly. Here, we demonstrate a method to assemble carbon nanotubes from solution on ferromagnetic contacts using a commercially available permanent magnet.

Experimental Section

(a) Fabrication of the Ferromagnetic Electrodes. As substrates for the magnetic assembly, two different electrode configurations were used: (1) photolithographically patterned 2×100 μm Ni electrodes on p-type Silicon, without electrical contact pads, and (2) commercially available interdigitated Pt microelectrodes with contact pads, on borosilicate glass with an interdigit gap of 5 μm (Abtech Scientific Inc, VA). The Pt electrodes were modified by electrodepositing Ni and Co on the alternating electrodes. For the electrodeposition, electrolyte composition of the nickel and cobalt plating solutions were 1.0 M $NiCl_2$ + 1 M $CaCl_2$ and 1.0 M $CoCl_2$ + 1 M $CaCl_2$, respectively. The solution pH was adjusted to 0.3 by addition of HCl or NaOH. Electrodeposition was carried out at room

† Part of the special issue Frank H. Stillinger Festschrift".
* Address correspondence to these authors.
‡ Department of Chemistry.
§ Department of Chemical and Environmental Engineering.
|| Center for Nanoscale Science and Engineering.
⊥ Department of Physics.

10.1021/jp047156w CCC: $27.50
Published on Web 12/16/2004

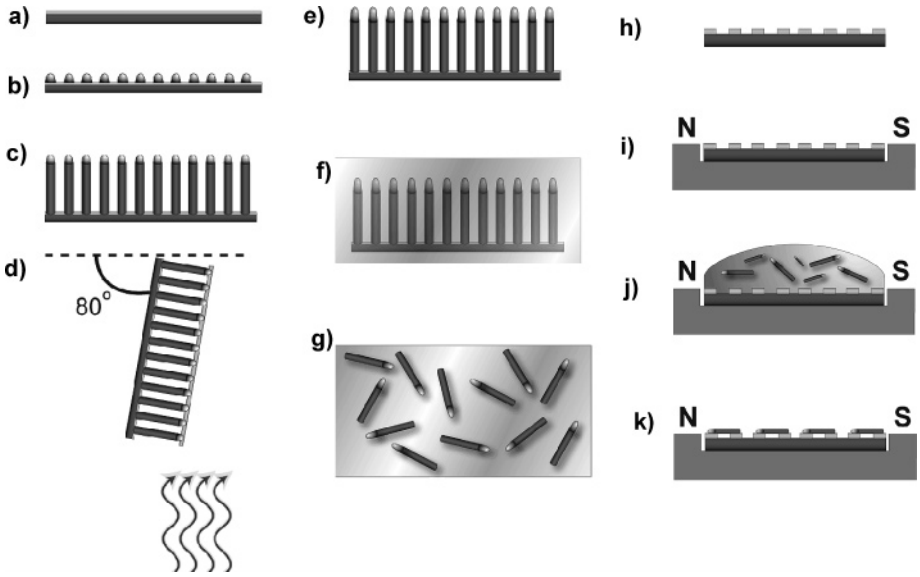

Figure 1. Schematic illustration of the fabrication and assembling process: (a) Silicon wafer with 10-nm-thick layer of catalyst; (b) catalyst islands on the silicon wafer; (c) MWNT growth (d) thermally evaporating a Ni cap on the MWNTs; (e) thermally reforming the magnetic caps; (f) amine adsorption on the MWNT walls; (g) MWNT dispersed in solution; (h) photolithographically patterned Ni lines on Si; (i) the chip is placed in a magnetic field; (j) The MWNT dispersion is allowed to dry on the magnetic lines; (k) MWNTs align to the magnetic field.

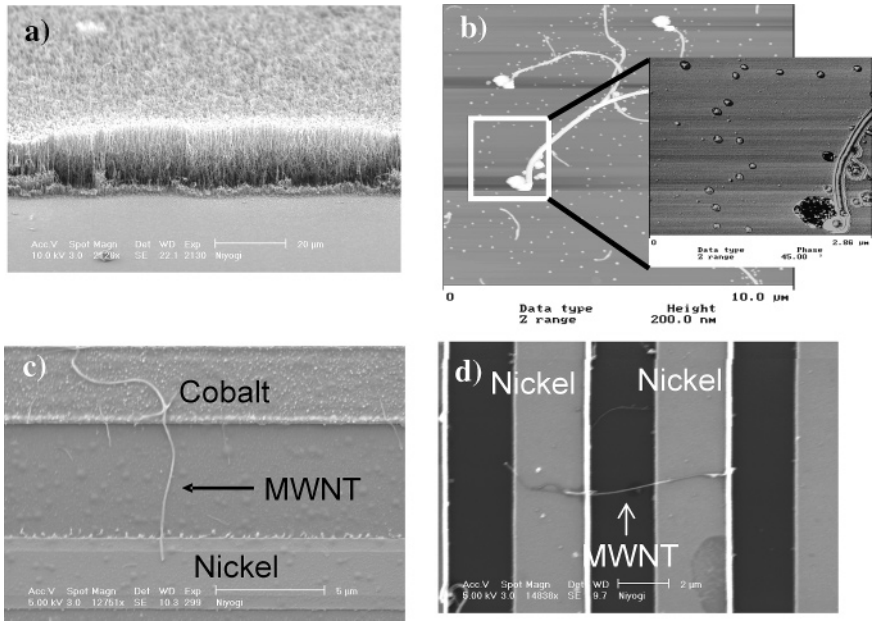

Figure 2. (a) CVD grown MWNTs on Si substrate with thermal evaporated Ni cap; (b) AFM image of the individually dispersed MWNTs in DMF; (c) SEM image of an individual MWNT assembled on electrochemically deposited Ni and Co electrodes on glass substrate, with an interelectrode gap of 5 μm; (d) SEM image of an individual MWNT assembled across Ni electrodes on Si.

temperature with current densities of 10 mA cm^{-2}. It is possible to control the thickness of the magnetic layer deposited by controlling the deposition time; in the data presented here, a 1-μm-thick layer was formed in 10 min of deposition.

(b) Carbon Nanotube Growth. MWNTs were grown on p-type B doped Si substrates under catalytic CVD conditions. The Si substrates were not etched to remove the native oxide layer. The presence of the SiO_2 layer prevents the formation of $FeSi_2$, which in turn prevents nanotube growth.[1,39] Ten nanometers of Fe was deposited on the substrate using vacuum thermal deposition. The substrate was then transferred into a quartz tube housed within an electrical tube furnace. The chamber was ramped to the growth temperature of 850 °C under Ar and H_2 at flow rates of 2.0 and 1.0 SLM, respectively. The catalyst pretreatment involved a 10-min reaction at 850 °C with NH_3 and H_2 at flow rates of 0.2 and 1.0 SLM, respectively (Figure 1b). The ammonia pretreatment has been shown to break up the catalyst film into islands with diameters which depend on the initial thickness of the catalyst layer.[40,41] The diameter of these islands directly influences the diameter and length of the nanotube's growth.[42] C_2H_2 at a flow rate of 0.05 SLM was used to initiate the growth of MWNTs. The growth was continued for 10 min after which the chamber was cooled to room temperature under Ar. This procedure leads to MWNTs that are vertically aligned with heights of 10−15 μm and diameters of 20−60 nm.

(c) Magnetic Assembly Technique. Figure 1 summarizes the fabrication steps that were used to create magnetically aligned carbon nanotubes. A 50-nm Ni layer was then evaporated with an angle of inclination of 10° onto the vertically

grown MWNTs to restrict the deposition to the top surface. Figure 2a shows an SEM micrograph of the vertically aligned MWNTS with the nickel nanomagnet cap in place. The substrates were then soaked in hexylamine overnight (Figure 1e), after which the nanotubes were dispersed in *N*,*N*-dimethylformamide (DMF) by using bath sonication for 30 min. The metal cap is visible at the ends of some of the MWNTs under AFM obtained from dispersions of the processed MWNTs. (Figure 2b). Only the longest nanotubes are expected to be capped with metal since the shorter tubes are not exposed at the top surface. The spherical particles of ~20 nm diameter observed in the AFM images are the remnant Fe catalyst particles. The aggregation of these particles at the tip of the MWNT (Figure 2b, inset) happened because the AFM sample was prepared under a magnetic field to observe any alignment in the absence of the microelectrodes. These particles assemble at the edges of the Ni electrodes under the influence of the magnetic field (Figure 2c). When a drop of the MWNT dispersion was allowed to evaporate on the Ni/Co electrodes in the presence of a permanent magnet ($H = 300$ Oe), the nanotubes were aligned with the field and became immobilized on the ferromagnetic contacts as the solvent evaporated (Figure 1k). The magnetic alignment of the nanotubes in the presence of the field was observed in situ using a video microscope (Hirox MX-10C 3-D).

(d) Characterization. Scanning electron microscopy (SEM) was performed on a Philips XL30 FEG instrument. A Digital Instruments Nanoscope IIIa was used for the atomic force microscopic (AFM) analysis of the devices. The dc-transport measurements were carried out in a flow cryostat at a base pressure of 10^{-6} torr. using a Keithly picoammeter.

Results and Discussion

In Figure 3, we demonstrate that the external magnetic field controls the assembling of the nanotubes on the magnetized Ni electrodes. When a drop of the nanotube dispersion is allowed to evaporate on the magnetic electrodes, the nanotubes reorganize under the effect of the field and in Figure 3a and b, we show that they assemble exclusively along the field direction at the edges of a 40-μm Ni strip. MWNTs do not assemble at the top edges and a relatively large density at the sharp corners can be attributed to a larger flux. This degree of alignment is comparable to those grown by the "kite mechanism" for short (10−15 μm) single-walled carbon nanotubes.[43] In Figure 3c, a relatively large concentration of nanotubes assembles across an array of electrodes, preferentially along the field direction. To obtain the larger density of individual nanotubes, the deposition process at the concentration used to obtain individual tubes across the whole length of the electrodes (Figure 2c, d) was repeated three times successively. Under these conditions, van der Waals and magnetic dipole interactions between the assembled and dispersed nanotubes tend to overcome the aligning forces on the individual tubes by the external field. To assemble independently addressable nanotubes with ferromagnetic contacts, this ability to guide the assembly using the external field removes the constraints of complicated lithographic processes and gives us the flexibility to tailor the ferromagnetic electrode properties.[44]

When the concentration of the nanotubes in the dispersion is increased, van der Waals interaction between the nanotubes force aggregation into networks and precipitation during solvent evaporation.[45] By comparing the morphology of the MWNT networks that evaporated on the bare Si substrate (Figure 4a)

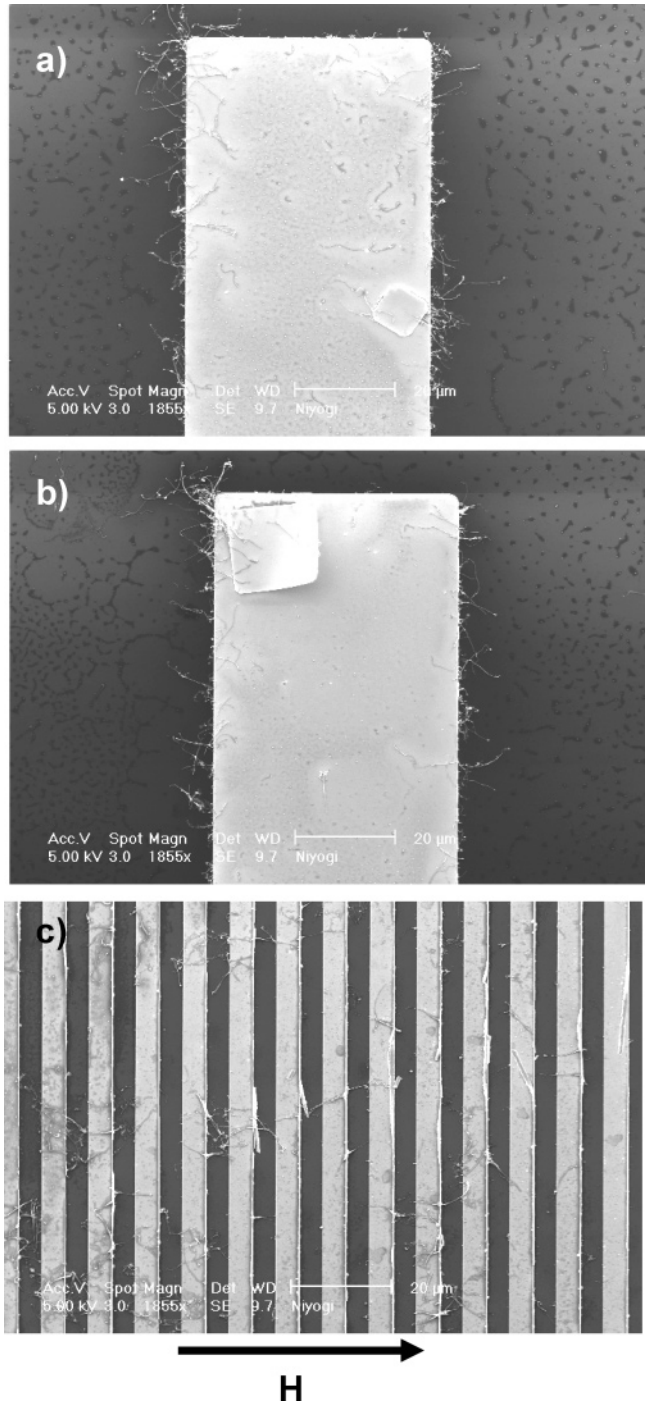

Figure 3. SEM image of magnetically assembled MWNTs on 40-μm Ni electrodes, showing the absence of any assembled nanotubes against the field direction at the top edge of the electrodes (a and b) and at the 5-μm electrode region of the same substrate (c).

next to the Ni electrode array (Figure 4b), a distinct effect of the magnetic field in the assembly can be seen. While on the Ni electrodes, the network is clearly elongated along the magnetic field direction; in the absence of such local concentration of the external field, the network spreads out in all directions. However, at even higher concentrations (Figure 4c), the MWNT bundles can exceed the limiting dimensions and the externally applied force is no longer able to influence any appreciable torque to align them.[46] By controlling the concentration of MWNTs in DMF, it is possible to obtain single nanotubes which bridge two magnetized pads (Figure 4d). It was also observed that solvent evaporation close to the aligned nanotube

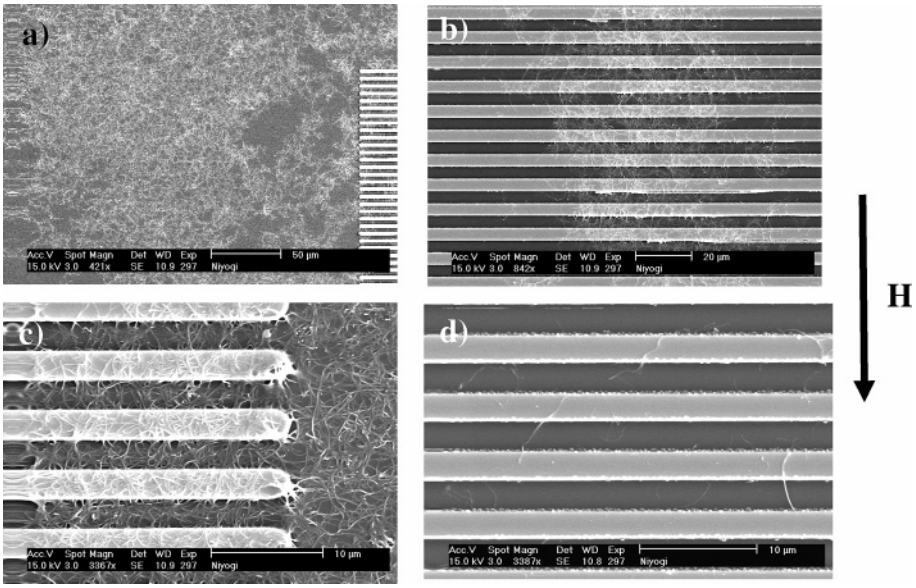

Figure 4. SEM images of assembled MWNTs across Ni electrodes on Si substrates showing the effect of concentration on the assembling process; (a) on bare Si; (b) on the electrode array where the magnetic flux is strong enough to align the network of nanotube bundles; (c) in a region of the electrodes where the concentration effect overcomes the external torque; (d) dilute dispersions allow assembling the MWNTs individually.

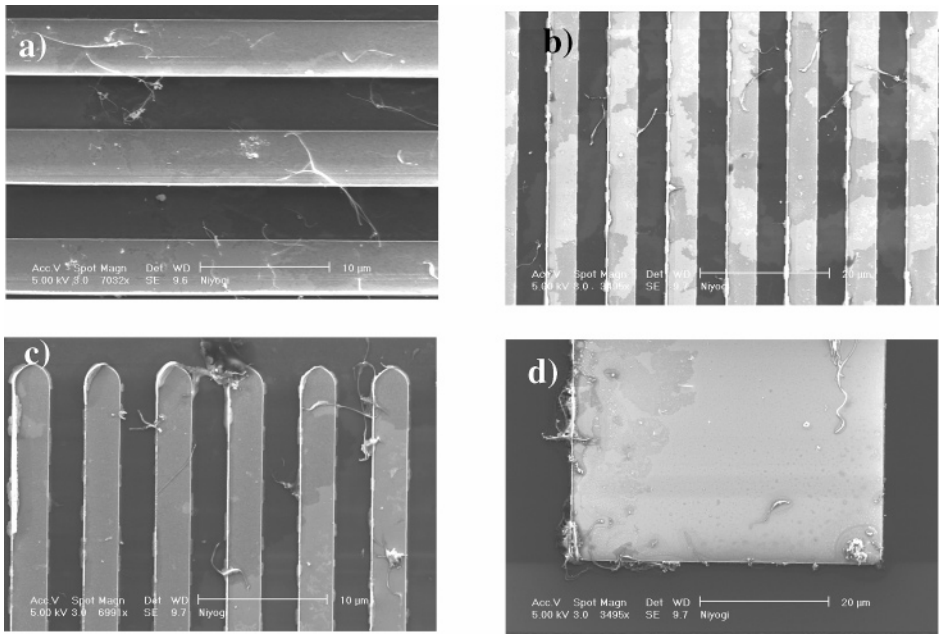

Figure 5. SEM image of MWNTs (dilute concentration) assembled without the external magnetic field (a, b, c); (d) the nanotubes now deposit on all edges of the large Ni electrode.

walls can force the flexible nanotubes to bend, within the plane of the substrate. Unlike previous reports on Ni nanowires, the MWNTs did not assemble in a head-to-tail chain geometry.[47]

The externally applied magnetic field of 300 Oe magnetizes the Ni electrodes, and this concentrates the magnetic flux in the region between the ferromagnetic electrodes. Since the force experienced by the ferromagnetic cap on the MWNTs in the presence of the magnetic field drives the assembly, it is expected that the size and shape anisotropy of the caps will control the MWNT alignment. The catalyst used for carbon nanotube growth (most commonly Fe, Ni, Co) remains attached to the nanotubes as nanoparticles. Depending on the growth conditions, these nanoparticles can remain attached to the root or the tip of the nanotube, or multiple nanotubes can grow three-dimensionally from a single catalyst particle.[1,48,49] This residual catalyst was recently used to assemble single-walled carbon nanotubes under external magnetic fields.[38] Our procedure for adding an additional ferromagnetic cap on the nanotubes allows us to tailor the magnetic contact between the nanotube and the electrodes as well as to exploit the advantages of nanoscale magnetic materials. In these experiments, a 50-nm Ni cap was thermally evaporated which would result in an aspect ratio of 1, compared to the much larger aspect ratio (10^3) of the MWNTs. By increasing the aspect ratio of the ferromagnetic caps, an easy axis for magnetization can be established along the MWNT axis and the coercive fields at the ends of the MWNTs can be controlled. Capping both ends of the nanotube in this manner will ensure greater control over the alignment process.

In the absence of any applied magnetic field (Figure 5), the MWNTs adopt a random orientation. The effect is most evident on comparing Figure 3a and b with Figure 5d. The deposition in the absence of the magnetic field was carried out only once so that the concentration of the sample was one-third of those in Figure 3.

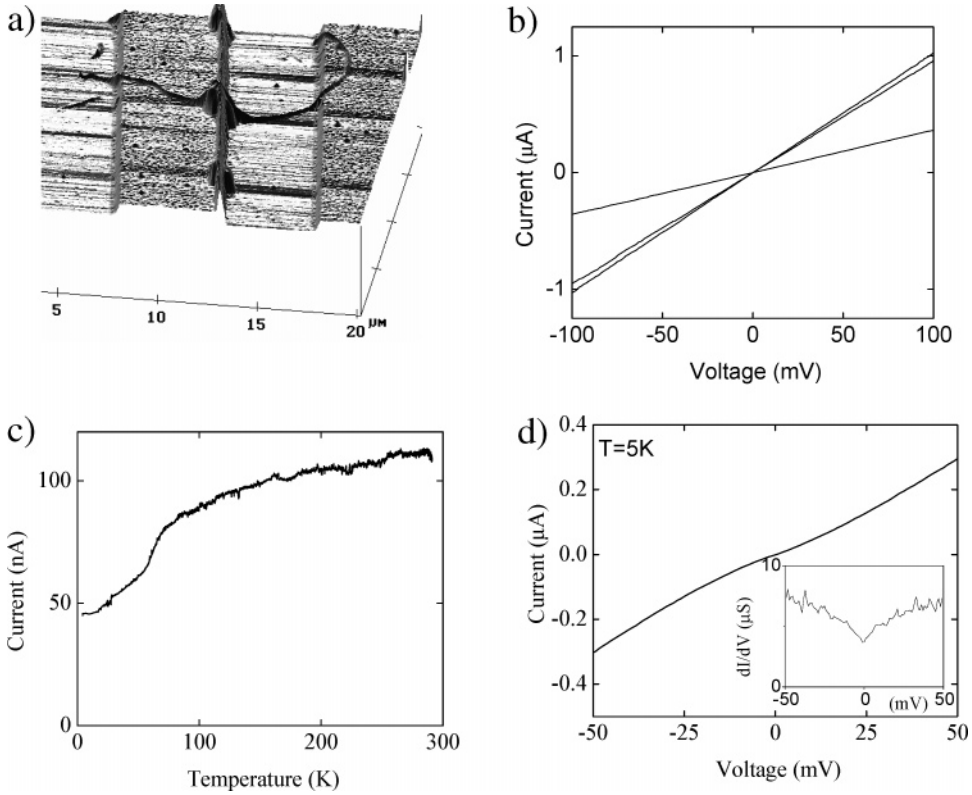

Figure 6. (a) AFM image of a typical device showing the contour of the MWNT on the Ni electrode surface. The nanotube sits on the Si surface rather than hanging across the electrodes; (b) $I-V$ (current−voltage) characteristics of MWNTs at room temperature for three devices; (c, d) the low-temperature behavior of the transport properties of a device.

The fabrication process allows us to use any combination of ferromagnetic materials either as the contacts or as the MWNT caps.[50] The use of asymmetric contacts (Figure 2c) is particularly beneficial for spin transport related measurements, since the magnetoresistance at the two terminals can then be controlled using the externally applied field.[19]

To characterize the electrical transport properties of the assembled devices, commercial electrodes patterned on glass with large contact pads were used. Figure 6a shows a typical AFM 3D height image of a device prepared by the magnetic assembly technique showing the contour of the MWNT on the Ni electrodes. The electrical properties of the devices are investigated by two-point conductance measurements. Current versus voltage ($I-V$) characteristics are obtained by applying a dc voltage across the sample and measuring the current with a digital picoammeter. All samples investigated show a linear $I-V$ curve at room temperature, which indicates the formation of ohmic contacts. Figure 6b shows the $I-V$ curves of three devices with resistance values of 98 kΩ, 105 kΩ, and 276 kΩ. The variation in resistance could be due to several factors. First, a device fabricated on interdigitated electrodes may consist of more than one nanotube spanning the two electrodes. As discussed above, we have observed that the number of nanotubes can be controlled by adjusting the concentration of the dispersion. A second factor is the contact resistance, which is often the dominant resistance in nanotube devices.[51,52] In the present two-point measurement geometry, the contact resistance cannot be isolated. Suitable modification of the electrode geometry will enable four-point measurements to determine the sample-to-sample variation in contact resistance in future studies.

Figure 6c shows the temperature dependence of the sample current for the device, when a fixed voltage of 10 mV is applied. The device in Figure 6c exhibits semiconducting behavior: the current increases (i.e., the resistance decreases) as the temperature increases.

To understand the low-temperature behavior, we measure sample current (I) as a function of voltage at $T = 5$ K (Figure 6d) and obtain the differential conductance (dI/dV) by numerical differentiation (Figure 6d, inset). In contrast to the linear $I-V$ curves at room temperature, the low-temperature $I-V$ curve is nonlinear. This is most apparent in the differential conductance data (Figure 6d, inset) which exhibit a dip in conductivity at zero voltage. This behavior is consistent with CNT devices fabricated by other methods, such as e-beam lithography with gold contacts on top of dispersed CNT,[53] CVD growth from patterned catalysts,[27] e-beam lithography with CNT on top of contacts,[54] and CNT with ferromagnetic contacts.[30] At sufficiently low temperatures, some of these devices exhibit a complete suppression of conductivity at zero bias known as Coulomb blockade. Others have observed Luttinger liquid like behavior.[31,32]

For spin-based electronics, the important figure of merit is the magnetoresistance (MR) associated with the relative alignment of the magnetizations of the two ferromagnetic contacts, often referred to as giant magnetoresistance (GMR)[55] or the spin-valve effect. If spin-polarization is maintained as electrons are transported through the nanotube, a sharp change in resistance occurs when the relative alignment of magnetic contacts switches from parallel to antiparallel, and vice versa. This type of MR has been observed in ferromagnetically contacted CNT, with MR values ranging from 2 to 9% at low temperature (<10 K).[15,29,30,32] Other types of MR have been observed in CNT, such as negative MR at high magnetic fields ∼5 T,[27] but these are generally related to orbital motion, not GMR effects.

To measure MR associated with spin-polarized transport, we construct CNT devices contacted by two different ferromagnetic

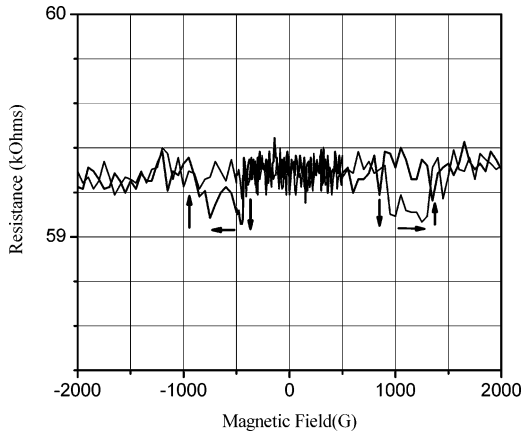

Figure 7. Magnetoresistance measured at $T = 2$ K on a Ni/MWNT/Co samples with a MWNT length of 5 μm.

materials. Since different ferromagnetic materials have different coercivities (i.e., magnetization reversal fields), an external magnetic field can be used to independently switch the magnetizations of the contacts to realize the parallel and antiparallel alignments of the moments. Before the CNT are attached to the electrodes, Ni and NiFe layers are electrodeposited onto the two interdigitated electrodes. After the CNT are magnetically assembled, the electrical and magnetic contact between the MWNT and the ferromagnetic electrode are further improved by electrodepositing a second layer of Ni and Ni−Fe on top of the respective electrodes. To date, we have not observed any appreciable MR related to the spin-valve effect. We believe that the use of commercially available interdigitated electrodes with ~5-μm gap is the primary limitation to our studies of spin-polarized transport, and we have initiated a new study that utilizes electron beam lithography for fabricating custom electrodes. Because previous studies have set the spin-diffusion length at 300 nm, we should reduce the size of our devices. Thus, it is currently unclear whether the magnetic assembly technique is suitable for spin-based electronics, and future studies are needed to address this question.

Conclusion

By modifying one end of vertically grown MWNTs with a ferromagnetic material, we have shown that it is possible to direct individual carbon nanotubes with a weak external magnetic field to assemble on ferromagnetic metal electrodes and create ohmic contacts. We have shown that the density of the assembled nanotubes can be controlled by the concentration of the nanotubes in the dispersion. The electrical properties of CNT devices fabricated were measured. Semiconducting devices have been created with linear $I-V$ curves at room temperature and nonlinear $I-V$ curves at low temperatures, consistent with devices produced by other methods. Thus, we demonstrate a protocol for assembling carbon nanotubes at desired densities, which will allow evaluation of electronic charge- and spin-related transport phenomena in these chiral molecular conductors.

Note Added in Proof

We have recently observed a ~0.3% magnetoresistance effect (Figure 7) on a Ni/MWNT/Co (200 nm, electrodeposited over Ni) device assembled on Si, with a gap of 5 μm, at $T = 2$ K. A Quantum Design physical property measurement system was used to control the temperature and the magnetic fields for these measurements.

Acknowledgment. We would like to acknowledge the contribution of Mangesh Bangar in wire bonding samples for the magnetoresistance measurements. The work was supported by DOD/DARPA/DMEA under grant number DMEA90-02-2-0216.

References and Notes

(1) Dai, H. In *Topics in Applied Physics*; Dresselhaus, M. S., Dresselhaus, G., Avouris, P., Eds.; Springer-Verlag: Berlin, 2001; Vol. 80, pp 29−53.
(2) Zhang, Y.; Chang, A.; Cao, J.; Wang, Q.; Kim, W.; Li, Y.; Morris, N.; Yenilmez, E.; Kong, J.; Dai, H. *Appl. Phys. Lett.* **2001**, *79*, 3155−3157.
(3) Diehl, M. R.; Yaliraki, S. N.; Beckman, R. A.; Barahona, M.; Heath, J. R. *Angew. Chem., Int. Ed.* **2002**, *41*, 353−356.
(4) Huang, Y.; Duan, X.; Cui, Y.; Lauhon, L. J.; Kim, K.-H.; Lieber, C. M. *Science* **2001**, *294*, 1313−1317.
(5) Huang, Y.; Duan, X.; Wei, Q.; Lieber, C. M. *Science* **2001**, *291*, 630−633.
(6) Cui, Y.; Wei, Q.; Park, H.; Lieber, C. M. *Science* **2001**, *293*, 1289−1292.
(7) Melosh, N. A.; Boukai, A.; Diana, F.; Gerardot, B.; Badolato, A.; Petroff, P. M.; Heath, J. R. *Science* **2003**, *300*, 112−115.
(8) Bentley, A. K.; Trethewey, J. S.; Ellis, A. B.; Crone, W. C. *Nano Lett.* **2004**, *4*, 487−490.
(9) Iijima, S. *Nature* **1991**, *354*, 56−58.
(10) Hamada, N.; Sawada, S. I.; Oshiyama, A. *Phys. Rev. Lett.* **1992**, *68*, 1579−1581.
(11) Ramirez, A. P.; Haddon, R. C.; Zhou, O.; Fleming, R. M.; Zhang, J.; McClure, S. M.; Smalley, R. E. *Science* **1994**, *265*, 84−86.
(12) Ajayan, P. M. *Chem. Rev.* **1999**, *99*, 1787−1799.
(13) Mehrez, H.; Taylor, J.; Guo, H.; Wang, J.; Roland, C. *Phys. Rev. Lett.* **2000**, *84*, 2682−2685.
(14) Frank, S.; Poncharal, P.; Wang, Z. L.; de Heer, W. A. *Science* **1998**, *280*, 1744−1746.
(15) Tsukagoshi, K.; Alphenaar, B. W.; Ago, H. *Nature* **1999**, *401*, 572−574.
(16) Prinz, G. A. *J. Magn. Magn. Mater.* **1999**, *200*, 57−68.
(17) Wolf, S. A.; Treger, D. *IEEE Trans. Magn.* **2000**, *36*, 2748−2751.
(18) Dediu, V.; Murgia, M.; Mattacota, F. C.; Taliani, C.; Barbanera, S. *Solid State Commun.* **2002**, *122*, 181−184.
(19) Xiong, Z. H.; Wu, D.; Vardeny, Z. V.; Shi, J. *Nature* **2004**, *427*, 821−824.
(20) Ohgai, T.; Hoffer, X.; Gravier, L.; Wegrowe, J.-E.; Ansermet, J.-P. *Nanotechnology* **2003**, *14*, 978−982.
(21) Ren, Z. F.; Huang, Z. P.; Xu, J. W.; Wang, J. H.; Bush, P.; Siegal, M. P.; Provencio, P. N. *Science* **1998**, *282*, 1105−1107.
(22) Fan, S.; Chapline, M. G.; Franklin, N. R.; Tomber, T. W.; Cassell, A. M.; Dai, H. *Science* **1999**, *283*, 512−514.
(23) Murakami, Y.; Chiashi, S.; Miyauchi, Y.; Hu, M.; Ogura, M.; Okubo, T.; Maruyama, S. *Chem. Phys. Lett.* **2004**, *385*, 298−303.
(24) Cui, H.; Eres, G.; Howe, J. Y.; Puretkzy, A.; Varela, M.; Geohegan, D. B.; Lowndes, D. H. *Chem. Phys. Lett.* **2003**, *374*, 222−228.
(25) Dresselhaus, M. S.; Dresselhaus, G.; Eklund, P. C. *Science of Fullerenes and Carbon Nanotubes*; Academic: San Diego, CA, 1996.
(26) Collins, P. G.; Arnold, M. S.; Avouris, P. *Science* **2001**, *292*, 706−708.
(27) Hsiou, Y. F.; Yang, Y. J.; Stobinski, L.; Kuo, W.; Chen, C. D. *Appl. Phys. Lett.* **2004**, *84*, 984−986.
(28) Zhang, X. X.; Wen, G. H.; Huang, S.; Dai, L.; Gao, R.; Wang, Z. L. *J. Magn. Magn. Mater.* **2001**, *231*, L9−L12.
(29) Orgassa, D.; Mankey, G. J.; Fujiwara, H. *Nanotechnology* **2001**, *12*, 281−284.
(30) Kim, J.-R.; So, H. M.; Kim, J.-J.; Kim, J. *Phys. Rev. B* **2002**, *66*, 233401/1−233401/4.
(31) Zhao, B.; Monch, I.; Vinzelberg, H.; Muhl, T.; Schneider, C. M. *Appl. Phys. Lett.* **2002**, *80*, 3144−3146.
(32) Hoffer, X.; Klinke, C.; Bonard, J.-M.; Gravier, L.; Wegrove, J.-E. *Europhys. Lett.* **2004**, *67*(1), 103−109.
(33) Huang, S.; Cai, X.; Liu, J. *J. Am. Chem. Soc.* **2003**, *125*, 5636−5637.
(34) Gao, B.; Yue, G. Z.; Qui, Q.; Cheng, Y.; Shimoda, H.; Fleming, L.; Zhou, O. *Adv. Mater.* **2001**, *23*, 1770−1773.
(35) Cassavant, M. J.; Walters, D. A.; Schmidt, J. J.; Smalley, R. E. *J. Appl. Phys.* **2003**, *93*, 2153−2156.
(36) Garmestani, H.; Al-Haik, M. S.; Dahmen, K.; Tannenbaum, R.; Li, D.; Sablin, S. S.; Hussaini, M. Y. *Adv. Mater.* **2003**, *15*, 1918−1921.
(37) Lay, M. D.; Novak, J. P.; Snow, E. S. *Nano Lett.* **2004**, *4*, 603−606.
(38) Long, D. P.; Lazorcik, J. L.; Shashidhar, R. *Adv. Mater.* **2004**, *16*, 814−818.

(39) Cao, A.; Baskaran, R.; Frederick, M. J.; Turner, K.; Ajayan, P. M. *Adv. Mater.* **2003**, *15*, 1105−1109.

(40) Han, J.-H.; Lee, C. H.; Jung, D.-K.; Yang, C.-W.; Yoo, J.-B.; Park, C.-Y.; Kim, H. J.; Yu, S. G.; Yi, W.; Park, G. S.; Han, I. T.; Lee, N. S.; Kim, J. M. *Thin Solid Films* **2002**, *409*, 120−125.

(41) Chhowalla, M.; Teo, K. B. K.; Ducati, C.; Rupesinghe, N. L.; Amaratunga, G. A. J.; Ferrari, A. C.; Roy, D.; Robertson, J.; Milne, W. I. *J. Appl. Phys.* **2001**, *90*, 5308−5316.

(42) Teo, K. B. K.; Lee, S.-B.; Chhowalla, M.; Semet, V.; Binh, V. T.; Groening, O.; Castignolles, M.; Loiseau, A.; Pirio, G.; Legagneux, P.; Pribat, D.; Hasko, D. G.; Ahmed, H.; Amaratunga, G. A. J.; Milne, W. I. *Nanotechnology* **2003**, *14*, 204−211.

(43) Huang, S.; Woodson, M.; Smalley, R. E.; Liu, J. *Nano Lett.* **2004**, *4*, 1025−1028.

(44) Myung, N. V.; Nobe, K. *J. Electrochem. Soc.* **2001**, *148*, C136−C144.

(45) Bradley, K.; Gabriel, J.-C. P.; Gruner, G. *Nano Lett.* **2003**, *3*, 1253.

(46) Fischer, J. E.; Zhou, W.; Vavro, J.; Llaguno, M. C.; Guthy, C.; Haggenmueller, R.; Cassavant, M. J.; Walters, D. E.; Smalley, R. E. *J. Appl. Phys.* **2003**, *93*, 2157−2163.

(47) Tanase, M.; Silevitch, D. M.; Hultgren, A.; Bauer, L. A.; Searson, P. C.; Meyer, G. J.; Reich, D. H. *J. Appl. Phys.* **2002**, *91*, 8549−8551.

(48) Gavillet, J.; Loiseau, A.; Journet, C.; Willaime, F.; Ducastelle, F.; Charlier, J.-C. *Phys. Rev. Lett.* **2001**, *87*, 275504−275501−275504−275504.

(49) Gavillet, J.; Loiseau, A.; Ducastelle, F.; Thair, S.; Bernier, P.; Stephan, O.; Thibault, J.; Charlier, J. C. *Carbon* **2002**, *40*, 1649−1663.

(50) Myung, N. V.; Park, D.-Y.; Yoo, B.-Y.; Sumodjo, T. A. *J. Magn. Magn. Mater.* **2003**, *265*, 189−198.

(51) Dai, H.; Wong, E. W.; Lieber, C. M. *Science* **1996**, *272*, 523−525.

(52) Bezryadin, A.; Verschueren, A. R. M.; Tans, S. J.; Dekker, C. *Phys. Rev. Lett.* **1998**, *80*, 4036−4039.

(53) Bockrath, M.; Cobden, D. H.; McEuen, P. L. *Science* **1997**, *275*, 1922−1925.

(54) Tans, S. J.; Devoret, M. H.; Dai, H.; Thess, A.; Smalley, R. E.; Geerling, L. J.; Dekker, C. *Nature* **1997**, *386*, 474−477.

(55) Baibich, M. N.; Broto, J. M.; Fert, F.; Ngueyn Van Dau, F.; Petroff, F.; Etienne, P.; Creuzet, G.; Friederich, A.; Chazelas, J. *Phys. Rev. Lett.* **1988**, *61*, 2474−2475.